METHODS

Surface contrast enhancement of integumentary structures in X-ray tomography

Peter T. Rühr[1,2] (iD) and Markus Lambertz[3,4] (iD)

[1]*Institut für Zoologie, Universität zu Köln, Cologne, Germany*
[2]*Zentrum für Molekulare Biodiversitätsforschung, Zoologisches Forschungsmuseum Alexander Koenig, Bonn, Germany*
[3]*Institut für Zoologie, Rheinische Friedrich-Wilhelms-Universität Bonn, Bonn, Germany*
[4]*Sektion Herpetologie, Zoologisches Forschungsmuseum Alexander Koenig, Bonn, Germany*

Abstract

Micro-computed tomography (μCT) has become standard in the biological sciences to reconstruct, display and analyse 3D models of all kinds of organisms. However, it is often impossible to capture fine details of the surface and the internal anatomy at the same time with sufficient contrast. Here we introduce a new approach for the selective contrast-enhancement of integumentary surface structures. The method relies on conventional and readily available sputter coaters to cover the entire sample with a thin layer of gold atoms. This approach proved successful on a diverse array of plants and animals. On average, we achieved a 14.48-fold gain of surface contrast (ranging from 2.42-fold to 86.93-fold) compared with untreated specimens. Even X-ray-transparent samples such as spider silk became accessible via μCT. This selective contrast-enhancement, makes it possible to digitally reconstruct fine surface structures with low absorbance while the tissue-dependent grey value resolution of the inner anatomy is maintained and remains fully visualisable. The methodology is suited for a broad scientific application across biology and other sciences employing (μ)CT, as well as educative and public outreach purposes.
Key words: 3D morphology; reconstruction; sputtering; staining; volume render; μCT.

Introduction

The acquisition of accurate three-dimensional (3D) morphological data is a crucial prerequisite for many taxonomic, functional, comparative and developmental studies (Jones et al. 2009; Akkari et al. 2015; Blanke et al. 2015; Parapar et al. 2017; Schachner et al. 2017). Micro-computed tomography (μCT) accordingly has developed into a standard technique in biology for capturing internal and external information in 3D (Holdsworth & Thornton, 2002). Certain integumentary structures, such as insect wings and bird feathers, however, possess low inherent X-ray absorbance, frequently resulting in extremely low contrasts when scanned at commonly available X-ray source energies. While contrast-enhancement of *internal* soft tissues with various staining solutions has become an established and readily available approach in both zoology (Metscher, 2009; de S. e

Silva et al. 2015; Gignac et al. 2016) and botany (Dhondt et al. 2010; Karahara et al. 2015), no staining procedure exists specifically to enhance the contrast of delicate *external* structures. Difficulties in visualisation primarily are due to two factors: (1) the low absorption of X-ray photons by the surface structure, resulting in insufficient attenuation in tomographic projections, and (2) the sample contains other, more X-ray opaque components blocking the X-ray beam at the tube energy that is needed to achieve adequate contrast values in the less absorbent surfaces (so-called 'metal artefact', Barrett & Keat, 2004). Decreasing the source energy of the μCT-system to increase absorption is one option to solve the former problem. However, most X-ray sources have a low yield at lower energies (Hupfer et al. 2012), which drastically increases the required exposure time for each projection and thus introduces a higher risk of sample movement during scanning. This furthermore severely reduces sample throughput (du Plessis et al. 2017). Additionally, lower X-ray energies can, again, cause metal artefacts due to excessive absorption of other sample regions with higher X-ray density (Barrett & Keat, 2004; du Plessis et al. 2017). To circumvent these problems, we introduce gold-coating as a simple and efficient new approach specifically to enhance the contrast of integumentary

Correspondence

Peter T. Rühr, Institut für Zoologie, Universität zu Köln, Biozentrum, Zülpicher Straße 47b, 50674 Cologne, Germany. E: p.t.ruehr@ uni-koeln.de

surfaces. In principle, our new approach can be applied to all dry surfaces, not only those that are organismic.

Materials and methods

Samples

We analysed samples with a typically low X-ray contrast, ranging from plant seeds and various invertebrates to avian feathers. Plant samples include the seed of a dandelion *Taraxacum* sp. (Asterales: Asteraceae) and a seed filament of *Clematis* sp. (Ranunculales: Ranunculaceae). Invertebrate samples were a red-tailed bumblebee *Bombus lapidarius* (Linnaeus, 1758) (Hymenoptera: Apidae), a middle-barred minor *Oligia fasciuncula* (Haworth, 1809) (Lepidoptera: Noctuidae), a moth fly *Clogmia albipunctata* (Diptera: Psychodidae), a common fruit fly *Drosophila melanogaster* Meigen, 1830 (Diptera: Drosophilidae) cocooned in the web of a long-bodied cellar spider *Pholcus phalangioides* Füssli, 1775 (Araneae: Pholcidae), a part of an empty cocoon of the Socotra Island blue baboon tarantula *Monocentropus balfouri* (Araneae: Theraphosidae) spanned between two pipette tips, and an isolated pedipalp of the cellar spider *Artema nephilit* Aharon, Huber & Gavish-Regev, 2017 (Araneae: Pholcidae). A breast feather and a wing feather of the Eurasian blackcap *Sylvia atricapilla* (Linnaeus, 1758) (Passeriformes: Sylviidae) were included as vertebrate examples. All animals used for this study came from the uncatalogued and/or teaching collections of one of the authors' home institutions. The plant material was freshly collected in the 'Biodiversitätsgarten' of the Zoologisches Forschungsmuseum Alexander Koenig in Bonn, Germany.

Micro-CT scanning

Micro-CT scanning was carried out with a Skyscan 1272 desktop device (Bruker, Kontich, Belgium). The specific scan settings for all specimens are detailed in the electronic supplement (Table S1). The samples were dried prior to the scanning process, either by simple air drying or, in case of the *Artema* pedipalp, after dehydration in a graded series of ethanol and subsequent immersion in hexamethyldisilazane (HMDS) in order to prevent shrinkage of internal soft tissues. Each specimen was first scanned without any additional treatment (reference scan). The samples then were treated with the surface coating (detailed below) and scanned once again with identical settings as used for the reference scan.

Surface coating

To enhance the contrast of the integumentary structures, we coated each specimen with a thin layer of gold. We used a conventional sputtering device (Sputter Coater 108auto, Cressington Scientific Instruments, Watford, UK), which is normally utilised for the pretreatment of scanning electron microscopy (SEM) samples. Coating was performed for 240 s at a pressure of 0.15 mbar with an electric current of 29 mA. This resulted in a coating of approximately 100 nm thickness.

Visualisation

Thermal drift compensation and virtual section reconstruction were performed in NRECON 1.7 (Bruker, Kontich, Belgium). To achieve comparable virtual section reconstructions (backprojections), the minimum and maximum of the dynamic range was set to the same Hounsfield values for each sample pair before image stack reconstruction. Volume renderings were created in DRISHTI 2.6 (Limaye, 2012). Here, the lower margin of the transfer functions were defined just above the grey value of the background to visualise as much of the non-background signal as possible and to avoid user-biased results. The surface model of the *Artema* pedipalp cuticle was reconstructed in DRISHTI 2.6, and the surface model of the pedipalp musculature was created in ITK-SNAP 3.6 (Yushkevich et al. 2006). These two surface models were combined and rendered in BLENDER 2.79 (www.blender.org).

Down-sampled 8-bit image stacks of the coated and non-coated samples were made available on MorphoBank (O'Leary & Kaufman, 2012) under project number 3140 (http://morphobank.org/permalink/?P3140). Full resolution 16-bit stacks are available from the corresponding author upon reasonable request.

Quantification of the contrast ratio

Quantitative contrast analyses were performed on the original 16-bit TIFF images. We determined the Weber contrast C, which is defined as the difference of the sample intensity and the background intensity, divided by the background intensity (Eq. 1). We used the modal intensity value (the most common grey value, I_{Mod}) of the image to represent the background intensity, and the maximum intensity value of the image (I_{Max}) as the maximum intensity value of the sample.

$$C = \frac{I_{Max} - I_{Mod}}{I_{Mod}} \tag{1}$$

The C-values for each untreated sample were compared with the respective C values for the coated samples in order to evaluate the contrast gain, which is defined as the ratio between both values. A paired t-test was used to statistically compare C-values of the two groups.

To exclude overestimation of contrast values, we ensured that the image regions that were used for contrast measurements did not contain regions of excessively absorbing material by checking both the images themselves and their logarithmic histograms. The built-in 'Remove Outliers' rank filter of FIJI (Schindelin et al. 2012) was used (radius = 4 pixels, threshold = 50 grey values) on every 16-bit image before contrast measurements to eliminate noise.

Grey value measurements were performed in FIJI (Schindelin et al. 2012). Calculations, analysis and plotting was carried out with custom scripting in the R software environment (v. 3.4.3). Figures were composed in GIMP 2.8 (www.gimp.org) and final plates were created in SCRIBUS 1.5 (www.scribus.net). All software packages used in this study (except NRECON) are published under the GNU General Public License (GPL).

## Results and discussion

Choice of contrast measurement

Contrast is often measured using the Michelson contrast (Michelson, 1927), by which the total range between minimum and maximum intensity values in an image is measured. In computed tomography, however, adjacent materials with significant X-ray density differences often
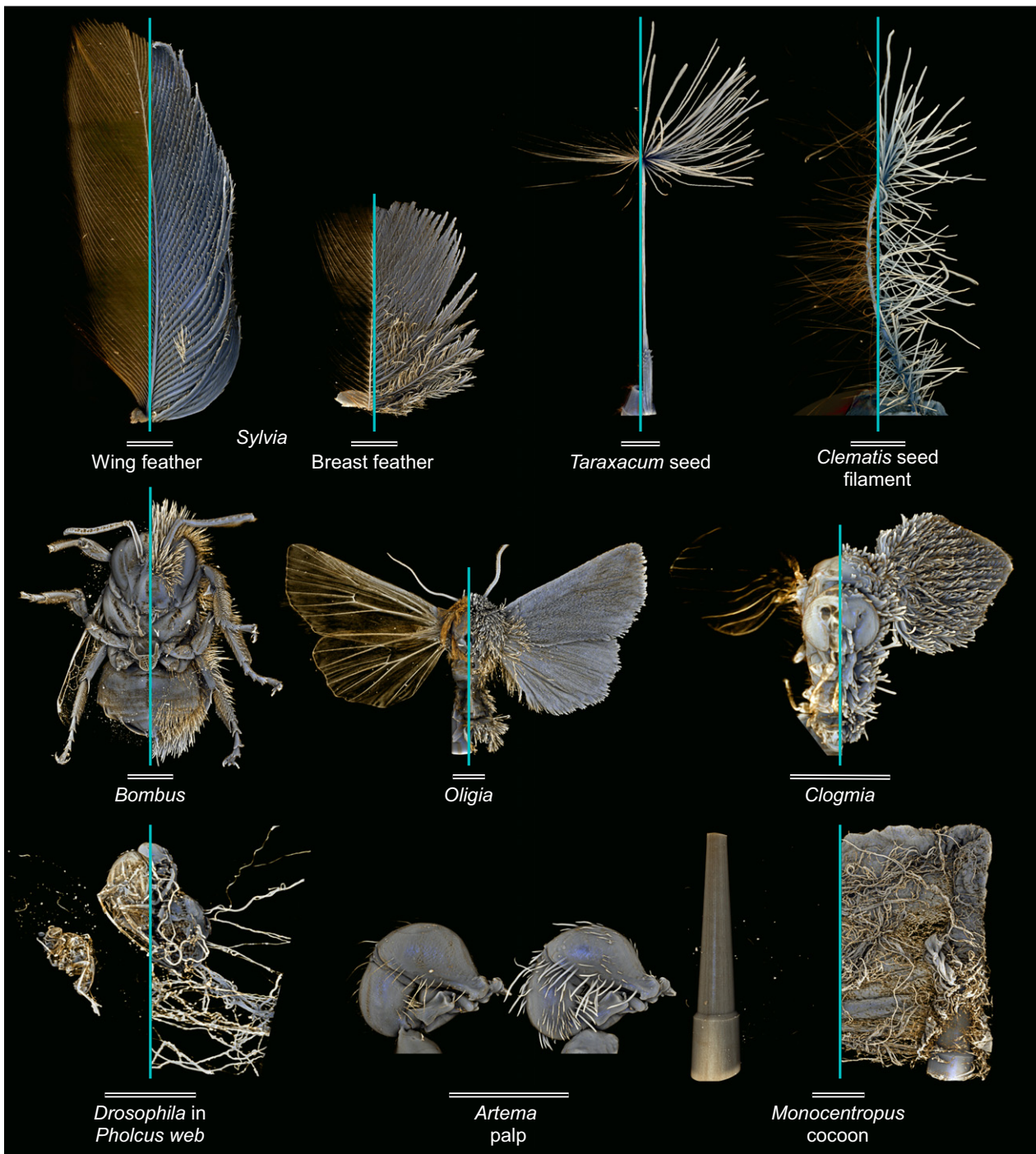
Fig. 1 Volume renderings of the studied samples, all revealing a substantial gain in morphological detail after coating. Left halves are non-coated, right halves are coated. In the case of *Artema* (lower middle), the whole sample is shown twice. Scale bars: 2 mm.

experience edge enhancements due to the differential refraction and thus phase shift of X-rays at the sample edges. This has the effect that bright areas in the backprojections, representing more X-ray-dense materials (e.g. insect cuticle) are often surrounded by a dark 'halo' of grey values that are lower than the surrounding background intensity (e.g. air). This becomes evident in the minima of the profile plot in Fig. 1c, which lie below the average background intensity. Although the Michelson contrast is suitable to quantify the contrast of images with a consistent background colour, it would lead to an overestimation of the actual contrast gain that is achieved by coating due to
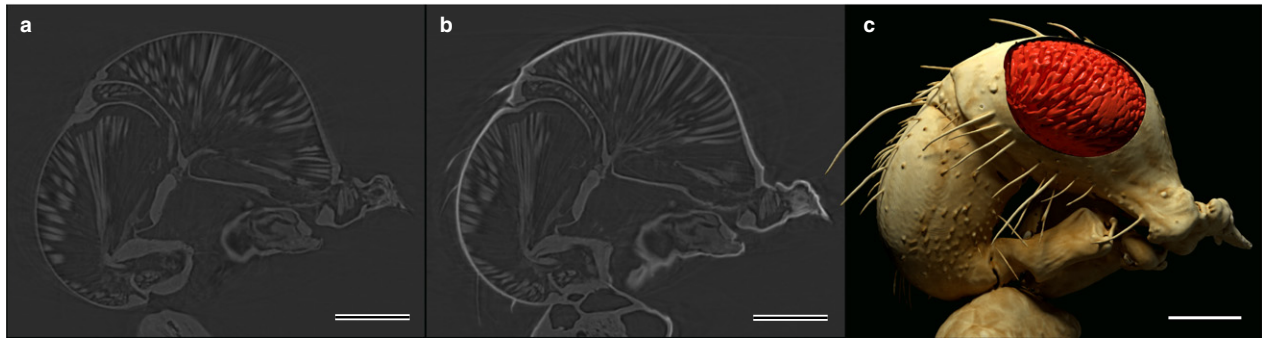
Fig. 2 Digital slice reconstructions of the pedipalp of *Artema* (a,b). Note the increased contrast of the integument in the coated sample (b), making the automatic, threshold-based extraction of a surface model (c) possible. A window was cut into the surface model of (c) to visualise the internal musculature and to demonstrate that capturing the internal morphology is not affected by the coating treatment. Scale bars: 0.5 mm.

the edge enhancement in tomography images as outlined above. Hence, we considered the Weber contrast C.

Contrast gain in volume renders and simplification of mesh extraction

An immense gain in information on integumentary details was revealed by the comparison of volume renderings of non-coated and coated samples (Fig. 1). These volume renderings are created by separating the sample from the background by simple grey-value thresholding. In all coated samples, even the most delicate structures become visible, whereas they were difficult or impossible to visualise in the non-coated samples.

This is because the coating technique reduces or removes signal overlap of the surface and background. It also increases the contrast of surface structures relative to internal tissues. Hence, it allows the automatic, threshold-based mesh extraction (Fig. 2) of the sample surface (e.g. cuticle), which, without coating, frequently has similar grey values in a μCT scan as internal anatomical structures (e.g. muscles). Although gold-coating adds an additional X-ray-absorbing layer to the exterior of the specimens, internal structures are not altered by this procedure. Coating thus enhances the contrast and visualisation potential of the surface, but comes at no information loss regarding the internal anatomy. In addition, contrast enhancement of internal tissues using established staining methods can still be achieved in combination with gold coating, as well as SEM investigations before or after μCT scanning.

## Quantitative assessment of contrast gain

Further analyses of the scan data reveal the contrast enhancement of all samples after this treatment also in a quantitative way (Fig. 3, Supporting Information Fig. S1). Figure 3a–d exemplarily details the effect on a wing feather of the Eurasian blackcap. The non-coated sample shows little grey-value change in the projections compared with the background. In contrast, there is strong absorption including

clearly recognisable individual peaks representing a much more discrete sample signal of the coated feather (Fig. 3a). A comparison of the histograms of both approaches (Fig. 3b) further demonstrates the gain in contrast of the projections vs. the background: the non-coated sample shows a single peak with a narrow frequency distribution and an overlap of background and sample signal, whereas two discrete peaks and a broader frequency distribution are characteristic for the coated one. Here, the attenuation signal of the feather is clearly separated from the background.

The effect of this informational gain for further downstream analyses becomes particularly evident in the backprojections of the μCT scans. The profile plot along the non-coated feather shows very low sample signal in relation to the background, compared with distinct grey-value changes along the coated feather (Fig. 3c). There is also a much wider range in the respective histograms (Fig. 3d). Contrast values in the backprojections of all coated samples are significantly higher ($P < 0.001$) than those of the non-coated samples (Fig. 3e,f), with an average 14.48-fold contrast improvement. In some specimens, such as the delicate spider silk samples, scanning without treatment resulted in a signal indistinguishable from the background noise, whereas coating with gold yielded high contrast values that allowed decent visualisation of the sample. All contrast gain values are listed in the supporting information (Table S2).

Partial volume effects

With a thickness of around 100 nm, the layer of gold on the samples is much smaller than the sizes of the reconstructed voxels, which range from 4.4 to 12 μm. Nevertheless, the gold layer is clearly visible in the scans. This is because the intensity of each voxel of a tomography scan represents the average attenuation of the material volume depicted by it. When the attenuation of tissues within such a material volume differs widely due to their highly disparate X-ray absorption properties (such as delicate integumentary structures vs. gold particles), the impact of material with extreme attenuation properties on the average
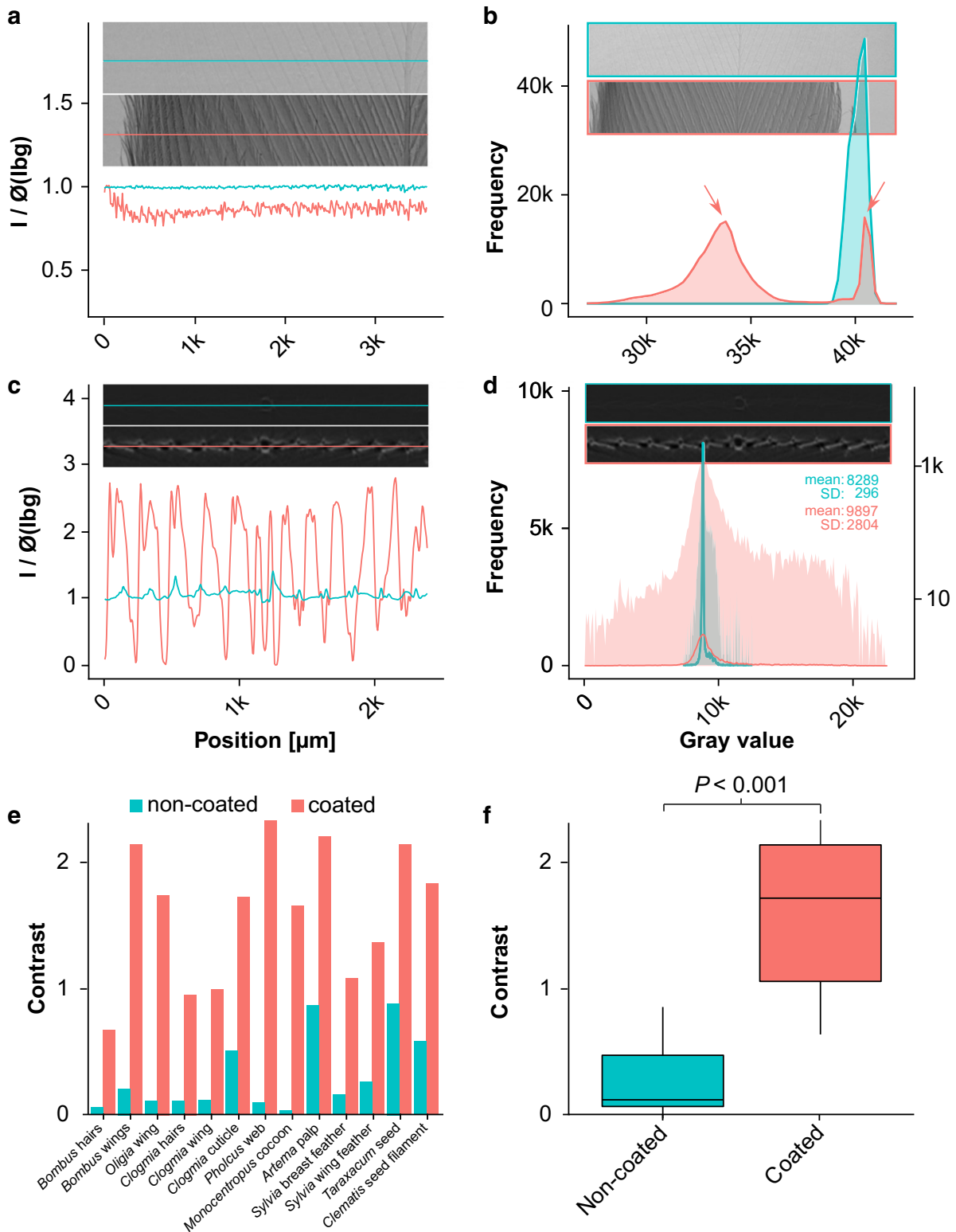
Fig. 3 Contrast comparison of the Eurasian blackcap wing feather projections (a,b) and backprojections (c,d). Normalised greyscale profiles are shown along the lines superimposed onto non-coated (cyan) and coated (red) samples. Histograms (b,d) visualise grey value frequencies of respective images. Red arrows: distinct peaks of coated sample signal (left) and background (right). Semi-transparent, logarithmic histograms are plotted in (d) on top of regular histograms illustrating the enlarged intensity range of the coated sample, also reflected by the increased standard deviation (SD) of grey values. (e) Mean contrast values of all non-coated and coated samples. (f) Two-paired *t*-test of the mean values of all non-coated and coated samples reveals highly significant contrast gains.

intensity of the voxel is strong. Additionally, voxel boundaries in tomography scans are always slightly blurred, so that even small objects can have an effect on several adjacent voxels. While this 'partial volume effect' has implications on fine-scale quantitative measurements near or below the voxel size of the scan, it also allows the extraction of data at scales below the actual scan resolution (Johns et al. 1993; Kinney et al. 1993). In the case of the present study, this effect allows the visualisation of delicate integumentary structures with otherwise insufficient attenuation after the application of a thin layer of gold.

Availability and potential applications

Gold-coating is already a widely available standard method used in both scientific and industrial SEM laboratories. To date, however, it has never been applied to μCT-scanning, even though impregnation with gold is known to be an effective staining method for internal soft tissue (Mizutani et al. 2007). Based on the highly significant contrast enhancement of sample vs. background after gold-coating, the practicability and accuracy of fast three-dimensional visualisation is considerably improved.

Different kinds of phase-contrast imaging techniques exist that increase the contrast of samples with low inherent absorbance (summarised by Diemoz et al. 2012). Although this approach is becoming more and more available in synchrotron-radiation-based setups and new generation desktop CTs, it does not distinguish between external surfaces and the internal tissue. Hence, our new approach provides the opportunity for any tomography setup to time-efficiently create surface representations of (biological) data that were not previously accessible. Given that the interior of the sample is not altered by the gold-coating, it furthermore allows the parallel (combined or separate) analysis of internal and external anatomy with a so far unmatched amount of detail. This methodological advancement consequently will be instrumental for a number of biological disciplines that depend on accurate morphological data of internal as well as external structures.

Areas of application that can employ such refined 3D reconstructions span the functionally motivated finite element analyses of insect wings to the fluid dynamic behaviour of their surrounding air masses, precise landmarking for geometric morphometric studies, and fundamental taxonomic assessments. The usability of this procedure, however, is not limited to a variety of strictly scientific applications, but additionally allows for the more effective presentation of complex biological data. Examples are 3D images, movies, 3D prints or virtual reality setups that can be used in an abundance of educative or information-oriented contexts – teaching, public outreach and museum environments. The recruitment of modern digital visualisation elements for these latter applications is becoming increasingly important, especially as the structures in question are difficult to grasp for non-trained persons based on 2D representations such as photographs or drawings.

Conflict of interest

The authors have no conflict of interest to declare.

Author contributions

P.T.R. and M.L. conceived the study, prepared the samples, wrote the paper. P.T.R. analysed the data.

References

Akkari N, Enghoff H, Metscher BD (2015) A new dimension in documenting new species: high-detail imaging for Myriapod taxonomy and first 3D cybertype of a new millipede species (Diplopoda, Julida, Julidae). *PLoS One* **10**, e0135243.

Barrett JF, Keat N (2004) Artifacts in CT: recognition and avoidance. *Radiographics* **24**, 1679–1691.

Blanke A, Rühr PT, Mokso R, et al. (2015) Structural mouthpart interaction evolved already in the earliest lineages of insects. *Proc R Soc B Biol Sci* **282**, 20151033.

Dhondt S, Vanhaeren H, Van Loo D, et al. (2010) Plant structure visualization by high-resolution X-ray computed tomography. *Trends Plant Sci* **15**, 419–422.

Diemoz PC, Bravin A, Coan P (2012) Theoretical comparison of three X-ray phase-contrast imaging techniques: propagation-based imaging, analyzer-based imaging and grating interferometry. *Opt Express* **20**, 2789–2805.

Gignac PM, Kley NJ, Clarke JA, et al. (2016) Diffusible iodine-based contrast-enhanced computed tomography (diceCT): an emerging tool for rapid, high-resolution, 3-D imaging of metazoan soft tissues. *J Anat* **228**, 889–909.

Holdsworth DW, Thornton MM (2002) Micro-CT in small animal and specimen imaging. *Trends Biotechnol* **20**, S34–S39.

Hupfer M, Nowak T, Brauweiler R, et al. (2012) Spectral optimization for micro-CT. *Med Phys* **39**, 3229–3239.

Johns RA, Steude JS, Castanier LM, et al. (1993) Nondestructive measurements of fracture aperture in crystalline rock cores using X ray computed tomography. *J Geophys Res Solid Earth* **98**, 1889–1900.

Jones AC, Arns CH, Hutmacher DW, et al. (2009) The correlation of pore morphology, interconnectivity and physical properties of 3D ceramic scaffolds with bone ingrowth. *Biomaterials* **30**, 1440–1451.

Karahara I, Yamauchi D, Uesugi K, et al. (2015) Three-dimensional imaging of plant tissues using X-ray micro-computed tomography. *Plant Morphol* **27**, 21–26.

Kinney JH, Breunig TM, Starr TL, et al. (1993) X-ray tomographic study of chemical vapor infiltration processing of ceramic composites. *Science* **260**, 789–792.

Limaye A (2012) Drishti: a volume exploration and presentation tool. *Proc SPIE 8506 Developments in X-Ray Tomography VIII*, 85060X. https://doi.org/10.1117/12.935640

Metscher BD (2009) MicroCT for comparative morphology: simple staining methods allow high-contrast 3D imaging of diverse non-mineralized animal tissues. *BMC Physiol* **9**, 11.

Michelson AA (1927) *Studies in Optics.* Chicago, IL: The University of Chicago Press.

Mizutani R, Takeuchi A, Hara T, et al. (2007) Computed tomography imaging of the neuronal structure of *Drosophila* brain. *J Synchrotron Radiat* **14**, 282–287.

O'Leary MA, Kaufman SG (2012) MorphoBank 3.0: Web application for morphological phylogenetics and taxonomy. Available: http://www.morphobank.org. Accessed 9 January 2017.

Parapar J, Candás M, Cunha-Veira X, et al. (2017) Exploring annelid anatomy using micro-computed tomography: a taxonomic approach. *Zool Anz J Comp Zool* **270**, 19–42.

du Plessis A, Broeckhoven C, Guelpa A, et al. (2017) Laboratory x-ray micro-computed tomography: a user guideline for biological samples. *Gigascience* **6**, 1–11.

de S. e Silva JM, Zanette I, Noël PB, et al. (2015) Three-dimensional non-destructive soft-tissue visualization with X-ray staining micro-tomography. *Sci Rep* **5**, 14088.

Schachner ER, Sedlmayr JC, Schott R, et al. (2017) Pulmonary anatomy and a case of unilateral aplasia in a common snapping turtle (*Chelydra serpentina*): developmental perspectives on cryptodiran lungs. *J Anat* **231**, 835–848.

Schindelin J, Arganda-Carreras I, Frise E, et al. (2012) Fiji: an open-source platform for biological-image analysis. *Nat Methods* **9**, 676–682.

Yushkevich PA, Piven J, Hazlett HC, et al. (2006) User-guided 3D active contour segmentation of anatomical structures: significantly improved efficiency and reliability. *NeuroImage* **31**, 1116–1128.

Supporting Information

Additional Supporting Information may be found in the online version of this article:

Fig. S1. Contrast comparison of the remaining samples studied, as detailed in Fig. 2a,b.

Table S1. Scan settings for all specimens studied. Note that these settings were kept identical for both scans performed on each specimen, i.e. non-coated and coated, respectively.

Table S2. Contrast gains of coated vs. non-coated specimens.